(2) Turro, N. J.; Gould, I. R.; Zimmt, M. B.; Cheng, C. C. *Chem. Phys. Lett.* **1985**, *119*, 484-488.
(3) Drake, J. M.; Levitz, P.; Turro, N. J.; Nitsche, K. S.; Cassidy, K. F. *J. Phys. Chem.* **1988**, *92*, 4680-4684.
(4) Levitz, P.; Drake, J. M.; Klafter, J. *J. Chem. Phys.* **1988**, *89*, 5224-5236.
(5) Even, U.; Rademann, K.; Jortner, J.; Manor, N.; Reisfeld, R. *Phys. Rev. Lett.* **1984**, *52*, 2164-2167.
(6) Bauer, R. K.; Mayo, P. d.; Natarajan, L. V.; Ware, W. R. *Can. J. Chem.* **1984**, *62*, 1279-1286.
(7) Bauer, R. K.; Mayo, P. d.; Okada, K.; Ware, W. R.; Wu, K. *J. Phys. Chem.* **1983**, *87*, 460-466.
(8) Krasnansky, R.; Koike, K.; Thomas, J. K. *J. Phys. Chem.* **1990**, *94*, 4521-4528.
(9) Bauer, R. K.; Mayo, P. d.; Ware, W. R.; Wu, K. C. *J. Phys. Chem.* **1982**, *86*, 3781-3789.
(10) Francis, C.; Lin, J.; Singer, L. *Chem. Phys. Lett.* **1983**, *94*, 162-167.
(11) Liu, X.; Iu, K.-K.; Thomas, J. K. *J. Phys. Chem.* **1989**, *93*, 4120-4128.
(12) Beck, G.; Thomas, J. K. *Chem. Phys. Lett.* **1983**, *94*, 553-557.
(13) Yang, C.; El-Sayed, M. A.; Suib, S. L. *J. Phys. Chem.* **1987**, *91*, 4440-4443.
(14) Albery, W. J.; Bartlett, P. N.; Wilde, C. P.; Darwent, J. R. *J. Am. Chem. Soc.* **1985**, *107*, 1854-1858.
(15) Scott, K. F. *J. Chem. Soc., Faraday Trans.* **1980**, *76*, 2065-2079.
(16) James, D. R.; Liu, Y. S.; Mayo, P. d.; Ware, W. R. *Chem. Phys. Lett.* **1985**, *120*, 460-465.
(17) James, D. R.; Ware, W. R. *Chem. Phys. Lett.* **1986**, *126*, 7-11.
(18) Basche, Th.; Brauchle, C. *J. Phys. Chem.* **1988**, *92*, 5069-5072.
(19) Basche, Th.; Sauter, B.; Brauchle, C. *Ber. Bunsenges. Phys. Chem.* **1989**, *93*, 1055-1058.
(20) Leheny, A. R.; Turro, N. J.; Drake, J. M. *J. Chem. Phys.*, in press.
(21) Klafter, J.; Blumen, A. *Chem. Phys. Lett.* **1985**, *119*, 377-382.
(22) Klafter, J.; Blumen, A. *J. Lumin.* **1985**, *34*, 77-82.
(23) Drake, J. M.; Klafter, J.; Levitz, P. *Science* **1991**, *251*, 1574-1579.
(24) Forster, T. *Discuss. Faraday Soc.* **1959**, *27*, 7-17.
(25) Tsai, T. E.; Griscom, D. L. *Phys. Rev. Lett.* **1991**, *67*, 2517.
(26) Leheny, A. R.; Turro, N. J.; Drake, J. M. Manuscript in preparation.
(27) Drake, J. M.; Levitz, P.; Klafter, J. *Isr. J. Chem.* **1991**, *31*, 135-146.
(28) Jackson, W. B.; Amer, N. M.; Boccara, A. C.; Fournier, D. *Appl. Opt.* **1981**, *20*, 1333.
(29) Tam, A. C. *Rev. Mod. Phys.* **1986**, *58*, 381.
(30) Devine, R. A. B. *Phys. Rev. Lett.* **1989**, *62*, 340.
(31) Tsai, T. E.; Griscom, D. L.; Friebele, E. J. *Phys. Rev. Lett.* **1988**, *61*, 444-446.
(32) Stathis, J. H.; Kastner, M. A. *Phys. Rev. B* **1984**, *29*, 7079-7081.

Condensation and Evaporation of H_2O on Ice Surfaces

D. R. Haynes, N. J. Tro,† and S. M. George*

Department of Chemistry and Biochemistry, University of Colorado, Boulder, Colorado 80309-0215
(Received: March 31, 1992; In Final Form: June 24, 1992)

The condensation and evaporation coefficients for H_2O on ice surfaces were measured using optical interference techniques. The condensation coefficient, α, was determined at ice surface temperatures from 20 to 185 K. For H_2O vapor at 300 K, the condensation coefficient decreased as a function of surface temperature from $\alpha = 1.06 \pm 0.10$ at 20 K to $\alpha = 0.65 \pm 0.08$ at 185 K. The temperature dependence of the condensation coefficient could be fit by a precursor-mediated adsorption model. The evaporation coefficient, γ, was obtained at various surface temperatures using isothermal desorption measurements. The evaporation coefficient was observed to be constant at $\gamma = 0.63 \pm 0.15$ for ice surface temperatures from 173 to 205 K. Over the temperature range where the condensation and evaporation coefficients could both be measured, α and γ were equivalent within the experimental error limits. This equivalence indicates that evaporation or condensation rates are dictated only by temperature and pressure and can be treated individually during net condensation, net evaporation, or steady-state equilibrium. An Arrhenius analysis of the H_2O isothermal desorption rates from ice at different temperatures revealed zero-order desorption kinetics expected for multilayer desorption. The activation barrier for desorption was $E_d = 11.9 \pm 0.2$ kcal/mol with a preexponential of $\nu_0 = 2.8 \times 10^{30} \pm 1.0 \times 10^{30}$ molecules/(cm^2 s). Quasi-equilibrium experiments also determined an enthalpy of sublimation for H_2O from ice of $\Delta H_{sub} = 11.8 \pm 0.2$ kcal/mol and an entropy of sublimation of $\Delta S_{sub} = 31.0$ cal/(K mol). The equivalency of the kinetic desorption barrier and the quasi-equilibrium enthalpy of sublimation indicates that there is no barrier for H_2O adsorption on ice surfaces. The measured condensation and evaporation coefficients predict the presence of polar stratospheric clouds over the Antarctic pole at 10-20 km. These measurements also reveal that ice surfaces in the polar stratosphere are very dynamic with H_2O condensation and evaporation rates of 10-1000 ML/s (1 ML = 9.8×10^{14} molecules/cm^2) for equilibrium conditions between 180 and 210 K.

I. Introduction

The condensation and evaporation of H_2O vapor on both liquid water and solid ice has been studied for many years.[1-9] Interest in this topic is motivated by its significance in understanding how processes such as cloud formation and growth occur in the atmosphere.[7,9-14] A detailed knowledge of the condensation and evaporation coefficients for H_2O on ice has increased in importance since recent atmospheric studies have revealed the role of heterogeneous chemistry on ice particles.[10] In particular, the ozone hole over Antarctica in the spring is intimately linked with the presence of ice particles known as polar stratospheric clouds.[15-17]

Modeling of heterogeneous chemistry in the stratosphere is dependent on accurate condensation and evaporation coefficients. Unfortunately, experimentally derived values of the condensation coefficient extend from approximately $\alpha = 0.01$[7,14,18] to $\alpha = 1.0$.[3,19-22] This considerable range of values can be attributed to the numerous techniques, experimental parameters, and theoretical assumptions that have been employed by the various studies. The temperature of the H_2O vapor and surface may also be very important, although no studies have established the dependence of the condensation coefficient on these parameters.

The condensation coefficient, α, and the evaporation coefficient, γ, are defined as

$$\alpha = C_{exp}/C_{max} \quad (1)$$

$$\gamma = E_{exp}/E_{max} \quad (2)$$

In these expressions, C_{exp} and E_{exp} are the experimental rates of condensation and evaporation, respectively. Likewise, $C_{max} = P_v(2\pi mkT_v)^{-1/2}$ and $E_{max} = P_s(2\pi mkT_s)^{-1/2}$ are the maximum theoretical rates of condensation and evaporation. P_v is the vapor pressure at temperature T_v, P_s is the vapor pressure that would be present for a system at equilibrium at a surface temperature

† Present address: Department of Chemistry, Westmont College, Santa Barbara, CA.

0022-3654/92/2096-8502$03.00/0

TABLE I: Known Evaporation Coefficient Measurements versus Temperature Using Evaporation and Heat Transfer Techniques

γ	temp range, K	method	ref
0.006–0.04	265–333	droplet evaporation	1, 18, 23, 24
0.02	373	liquid evaporation	28
0.045	293	liquid evaporation	30
0.94	188–213	ice evaporation	2
0.014–0.042	260–316	liquid evaporation	29
1.0	293–301	droplet evaporation	20
0.038	301–310	liquid evaporation	25
0.019	280	liquid evaporation	26
1.0	293	liquid evaporation	22
0.35–1.0	283–323	heat transfer	4
0.45–1.0	373	heat transfer	35
>0.1	298	heat transfer	33
1.0	298	heat transfer	21
0.2	323	heat transfer	34

TABLE II: Known Condensation Coefficient Measurements versus Temperature Using Direct Condensation Techniques

α	temp range, K	method	ref
unity	213–233	gravimetric	3
0.83 ± 0.15	133–158	gravimetric	5
0.06	193–223	ice crystal radial growth	11
$0.1 < \alpha < 0.50$	163–183	ice crystal radial growth	11
0.026	295–298	droplet radial growth	19
0.033	188–213	droplet radial growth	7
0.98	293	vapor loss	22
$0.8 < \alpha < 0.99$	138–152	gravimetric	36
$0.7 < \alpha <$ unity	280	vapor loss	8
0.04	293	liquid film growth	37
0.3 (+0.7, −0.1)	200	vapor flow loss	9
1.0 ± 0.1	150	IR absorption	38

T_s, m is the mass of the molecule, and k is Boltzmann's constant.

Early examinations of liquid water and solid ice surfaces focused on the evaporation of H_2O molecules and assumed that the condensation coefficient was equivalent to the evaporation coefficient.[1-3,12,18,19,23-29] However, this assumption of equality between condensation and evaporation coefficients has often been questioned.[5,31,32] A summary of the known evaporation experiments, results, and temperature ranges is presented in Table I.

A number of investigators have also measured the interfacial heat transfer resistance of condensing H_2O vapor at a liquid water surface.[4,21,33-35] All of these experiments have been performed at surface temperatures where H_2O evaporation could not be neglected. Consequently, determination of the condensation coefficients again required the assumption that condensation and evaporation coefficients were equivalent. The results of the various heat transfer measurements and their corresponding temperature ranges are given in Table I.

Techniques were developed more recently to measure condensation coefficients directly. Unfortunately, values for α from these direct measurements vary from $\alpha = 0.026$ to $\alpha = 1.0$.[3,5,7-9,11,19,22,36-38] A number of studies have utilized gravimetric methods to determine growth rates at an ice surface under a known H_2O vapor.[3,5,36] Additional experiments have measured pictographically the growth rates of ice crystals[11] and water droplets.[7] Other techniques based on vapor pressure variation in a closed system,[8] a fast flow reactor,[9] optical interference,[37] and Fourier transform infrared absorption spectroscopy[38] have also been implemented to measure α. The known investigations that have attempted to measure the H_2O condensation coefficient are listed in Table II.

In this paper, the condensation and evaporation coefficients of H_2O will both be measured accurately and independently with the use of an optical interference technique. In this optical interference method, reflected laser light produces interference fringes as the adlayer thickness changes on an optically flat substrate.[39-42] Hollenberg and Dows[39] originally established this method for the measurement of thin crystalline sample thicknesses. Groner et al.[40] later suggested this technique for the measurement of sticking coefficients, as well as for determining the growth of transparent matrix materials used in matrix isolation spectroscopy. Optical interference techniques have also been employed recently to measure rates of chemical vapor deposition,[41] laser-induced epitaxial crystallization,[43] bulk lattice temperature during laser annealing,[44] and molecular adlayer thicknesses.[45,46]

By use of the optical interference technique, the condensation coefficient of room temperature H_2O molecules colliding with an ice surface will be determined directly for substrate temperatures between 20 and 185 K. The evaporation coefficient will also be measured between 173 and 205 K. These studies will determine the kinetics and possible mechanisms of condensation and evaporation. The measurements will also establish whether the condensation and evaporation coefficients are equivalent away from equilibrium conditions as has been assumed in many previous studies. In addition, the investigations will determine if evaporation is significant above 170 K, where many experiments have measured condensation without considering evaporation. The isothermal desorption parameters will also be measured and the enthalpy and entropy of sublimation for ice multilayers will be determined under quasi-equilibrium conditions. These experimental measurements will provide the necessary information to model the growth and dynamic equilibrium of polar stratospheric clouds.

II. Experimental Section

A schematic diagram of the UHV chamber and experimental setup for this study has been shown elsewhere.[47,48] The UHV chamber was pumped by a 190 L/s Balzers turbomolecular pump, which was backed by another Balzers 50 L/s turbomolecular pump. After a bakeout, this tandem turbomolecular pump system yielded a base pressure of 5×10^{-10} Torr as measured by a Bayard-Alpert ion gauge. Additionally, the chamber was equipped with a UTI quadrupole mass spectrometer with a 1–300 amu mass range and 300 A/Torr sensitivity. The mass spectrometer was used for background gas analysis and temperature-programmed desorption.

Single crystals of $Al_2O_3(11\bar{2}0)$ were purchased from Saphikon. The Al_2O_3 crystal was mounted on a cold finger that was at the end of a double-vacuum-jacketed Dewar capable of holding liquid helium or liquid nitrogen. The $Al_2O_3(11\bar{2}0)$ surface was cleaned by heating to approximately 400 K with simultaneous exposure to an oxygen plasma discharge lasting at least 45 s.[49] This plasma process has been shown to produce clean Al_2O_3 surfaces.[49] A schematic diagram of the $Al_2O_3(11\bar{2}0)$ sample mounting technique has been previously shown.[50]

A film of tantalum with a thickness of 6000 Å was evaporated onto the back side of the $Al_2O_3(11\bar{2}0)$ sample. A clear window with a diameter of 0.25 in. remained at the center of the crystal. This arrangement allowed the crystal to be resistively heated by passing current through the tantalum film. Accurate crystal temperature measurement could be achieved with a chromel alumel thermocouple that was attached directly to the crystal with Ceramabond 569 high-temperature adhesive. The temperature was maintained by a temperature controller that could maintain temperatures to within ±0.5 K. Using liquid helium cooling, a temperature range from 20 to 700 K was obtainable.

Distilled and deionized water was obtained and placed in a cold finger attached to a gas handling line. Further purification of the water was implemented with several freeze–pump–thaw cycles. Specific backfill pressures of water vapor varying from 1.0×10^{-8} to 1.0×10^{-3} Torr could be introduced into the UHV chamber by employing a variable leak valve. The water vapor pressure was measured by the Bayard-Alpert ion gauge. Because ion gauge pressure readings are known to drift with time and their absolute sensitivities may be in error by as much as ±50%,[51] the ion gauge pressure was calibrated with an absolute MKS Barytron at pressures between 1.0×10^{-5} and 1.0×10^{-3} Torr. This calibration was linear and was subsequently extrapolated to calibrate the lower H_2O pressures employed in this investigation.

The typical condensation experiment involved raising the Al_2O_3 crystal to a specified temperature. A Uniphase He–Ne laser beam with a wavelength of $\lambda = 6328$ Å and an output power of 8 mW was incident on the $Al_2O_3(11\bar{2}0)$ surface at an angle of 22.5° off

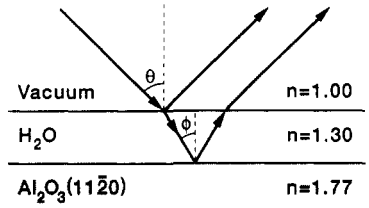

Figure 1. Optical geometry used for the HeNe laser interference measurements of the thickness of H_2O multilayers on $Al_2O_3(1120)$.

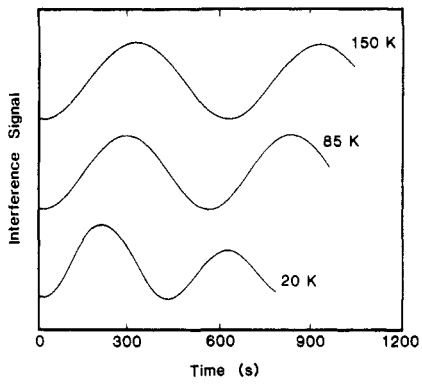

Figure 2. Reflectance of the incident HeNe laser beam as H_2O vapor at $P_v = 3.3 \times 10^{-6}$ Torr condenses onto an ice surface for various ice surface temperatures.

the surface normal. The laser beam was reflected from both the ice/vacuum interface and the ice/crystal interface as shown in Figure 1. These two reflections combined to form an interference signal. As the H_2O vapor deposited on the surface, the interference signal sinusoidally oscillated as the H_2O adlayer grew on the $Al_2O_3(11\bar{2}0)$ surface.

The interference signal was attenuated with a Schott NG-9 neutral density filter, measured by an EG&G FOD-100 photodiode, and digitized with a Stanford Research Systems Model 245 digitizer. The interference signal was at a maximum before H_2O deposition because only one reflection originates at the vacuum/$Al_2O_3(11\bar{2}0)$ interface. To study the condensation of H_2O on ice surfaces, the initial portion of the interference signal was ignored until the first minimum was attained. This first minimum corresponds to an H_2O multilayer with a thickness of approximately 1250 Å.

Isothermal experiments were used to determine the evaporation coefficients and the kinetic parameters for H_2O desorption from ice surfaces. In these studies, the substrate temperature was raised to a constant desorption temperature and the reflected interference signal was monitored as a function of time. As the H_2O molecules desorbed and the ice multilayer decreased in thickness, the reflection signal displayed a sinusoidally oscillating interference signal that was similar to the signals observed during condensation.

Quasi-equilibrium experiments were also performed by raising the Al_2O_3 substrate temperature and H_2O pressure simultaneously to maintain a constant H_2O multilayer thickness. Under these conditions, the condensation and desorption rates were equivalent and the reflected interference signal was held at a constant value. These are quasi-equilibrium conditions because as the substrate temperature changed, the gas temperature remained constant at $T_g = 300$ K.

III. Results

Figure 2 displays the interference signals versus time for three ice surface temperatures during condensation. The interference signals all begin at their first minimum. Because of the favorable change in the refractive index between vacuum, H_2O–ice, and Al_2O_3, the modulation depth was typically 90–95% of the peak of the reflected signal intensity. The traces were obtained by monitoring the He–Ne reflection from the vacuum/H_2O and $H_2O/Al_2O_3(11\bar{2}0)$ interfaces during H_2O adsorption. These experiments were performed at 5 K increments for surface temperatures from 20 to 185 K. The background H_2O pressures were $P_v = 3.3 \times 10^{-6}$ Torr for surface temperature between 20 and 165 K. In order to overcome H_2O desorption rates, the H_2O pressures were increased to $P_v = 8.2 \times 10^{-6}$ Torr at 170 K and to $P_v = 6.6 \times 10^{-5}$ Torr at 185 K. The faster oscillation frequency at lower surface temperatures displayed in Figure 2 indicates a more rapid H_2O multilayer growth rate and a higher condensation coefficient.

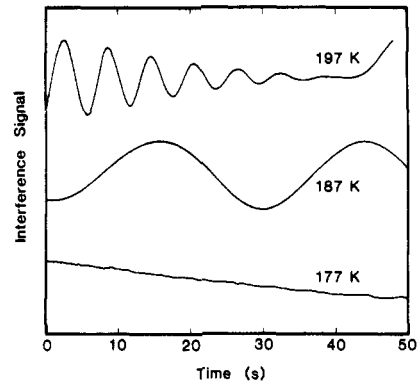

Figure 3. Reflectance of the incident HeNe laser beam as H_2O isothermally evaporates into vacuum from an ice surface for various ice surface temperatures.

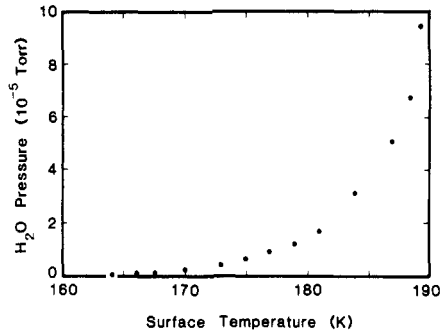

Figure 4. Relationship between the ice surface temperature and H_2O vapor pressure necessary to maintain a constant ice coverage. Condensation and evaporation rates are equivalent at these equilibrium H_2O vapor pressures.

Figure 3 shows the interference signals during the isothermal desorption of H_2O from ice multilayers at three surface temperatures. For these results, an H_2O multilayer was initially adsorbed on the $Al_2O_3(11\bar{2}0)$ surface. The temperature was then increased and the reflection was monitored when the sample reached the desired desorption temperature. These isothermal desorption experiments were performed at 2 K increments for surface temperatures from 173 to 203 K. The faster oscillation frequency at higher temperatures indicates a higher rate of H_2O desorption.

Figure 4 displays the steady-state relationship between the surface temperature and the corresponding H_2O vapor pressure required to keep the H_2O multilayer thickness at a constant coverage, i.e., an isosteric experiment. This quasi-equilibrium data were obtained by adjusting the substrate temperature synchronously with the background H_2O vapor pressure. Steady state was achieved when the reflected interference signal maintained a constant value.

IV. Discussion

A. Condensation Coefficient. The optical interference technique provides a convenient method to measure the H_2O multilayer thickness. Simple geometry yields the thickness of the H_2O multilayer corresponding to adjacent minima of the interference signal:

$$x = \lambda/2n_i(T) \cos \phi \qquad (3)$$

In this expression, x is the H_2O multilayer thickness required for one full period of the interference signal and $\lambda = 6328$ Å is the wavelength of the HeNe laser beam. Likewise, $n_i(T)$ is the tem-

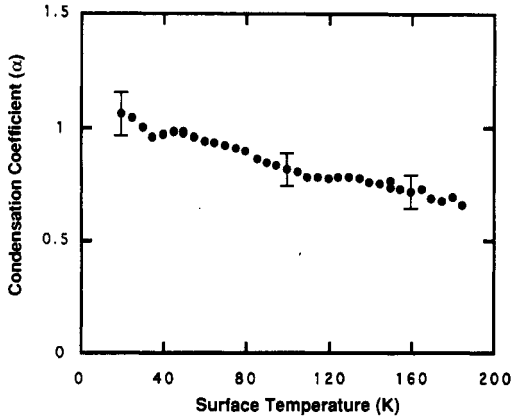

Figure 5. Condensation coefficient for H_2O on ice as a function of ice surface temperature.

perature-dependent index of refraction for ice.

As shown in Figure 1, ϕ is the laser angle of incidence relative to the Al_2O_3 surface normal. This angle is determined according to Snell's Law, $\sin\theta = n_i(T)\sin\phi$, where $\theta = 22.5°$ is the angle of incidence relative to the ice surface. The temperature-dependent refractive index for ice increases from $n_i = 1.32$ at 20 K to $n_i = 1.31$ at 185 K.[52] With these $n_i(T)$ values, ϕ changed from 16.9° to 16.7° and x varied from 2505 to 2521 Å.

The multilayer growth rate of the H_2O film is

$$dx/dt = \alpha P_v/[\rho(T)(2\pi mkT_g)^{1/2}] \quad (4)$$

where α is the condensation coefficient. As defined in eq 1, the condensation coefficient is the probability that an H_2O molecule colliding with the ice surface will be incorporated into the bulk. In addition, P_v is the H_2O vapor pressure, $\rho(T)$ is the temperature-dependent number density of the ice multilayer, $m = 18.016$ is the molecular weight of H_2O, and T_g is the impinging gas temperature. The temperature-dependent density of crystalline ice decreases from $\rho = 0.937$ g/cm^3 at 20 K to $\rho = 0.928$ g/cm^3 at 185 K.[52]

The multilayer growth rate, dx/dt, may be obtained from the interference signal versus time by employing eq 3. Subsequently, this multilayer growth rate can be equated with eq 4 and used to determine the condensation coefficient. At temperatures above 160 K, where desorption can be competitive with condensation, values for α were determined by using a modification of eq 4 that accounts for a finite evaporation rate:

$$dx/dt = \alpha P_v/[\rho(T)(2\pi mkT_g)^{1/2}] - [\upsilon_0/\rho(T)]e^{-E_d/RT_s} \quad (5)$$

In this relationship, υ_0 is the zero-order desorption preexponential, E_d is the desorption activation energy, and T_s is the ice surface temperature.

The condensation coefficients determined from temperature-dependent interference experiments such as those shown in Figure 2 are displayed in Figure 5. The condensation coefficient decreased linearly as a function of ice surface temperature from $\alpha = 1.06 \pm 0.10$ at 20 K to $\alpha = 0.65 \pm 0.08$ at 185 K. The error bars represent a propagation-of-errors analysis using the uncertainties in the measurements that are given below.

Condensation coefficients of $\alpha > 1$ are not physically possible. We believe that $\alpha \approx 1$ at 20 K and attribute our slightly larger α values to a number of possible experimental errors. These experimental errors and their approximate uncertainties are as follows: time base during interference measurements (±1%); visual fit of sinusoidal interference signals limited by analog/digital resolution (±2–3%); absolute Barytron pressure magnitude (±0.1%); calibration of the ionization gauge using the absolute Barytron and subsequent extrapolation to lower pressures (±7%); and the angle of incidence of the laser (±2%).

The measured condensation coefficients correspond well with some values given in Table II determined from direct condensation studies. However, other α values are significantly below the values obtained in this study. These lower condensation values may be attributed to competitive evaporation, because these measurements were typically performed at temperatures above 170 K, where ice multilayer desorption rates are appreciable.

Our condensation measurements were dependent on the assumption that the temperature-dependent H_2O multilayer density is equal to the density of crystalline ice I. However, ice has several structures that are dependent on the adsorption temperature. Vitreous ice forms below 113 K, ice I_c forms above 113 K and below 133–153 K, and ice I forms above 133–153 K and below 143–203 K.[52] The H_2O multilayer density is probably somewhere between the density of crystalline ice I and supercooled water. Supercooled water densities have been measured down only to 239 K.[53,54] The density for supercooled water decreases with decreasing temperature and the value at 239 K is $\rho = 0.978$ g/cm^3. In contrast, the density of crystalline ice I increases with decreasing temperature and is $\rho = 0.922$ g/cm^3 at 239 K.[52] Consequently, the densities of crystalline ice I and supercooled water are converging at temperatures less than 239 K and their differences are estimated to be ≤6%.

Condensation coefficients that decrease with increasing temperature have been observed for reactive sticking on single-crystal surfaces.[55,56] A decrease in the condensation rate with increasing surface temperature is consistent with a precursor-mediated adsorption mechanism.[57–59] In a precursor mechanism, initial adsorption occurs when an incident molecule is trapped on the surface in a weakly physisorbed state determined by van der Waals dispersion interactions. The incident physisorbed molecule can then either desorb back into the gas phase or incorporate itself into the surface.

The precursor-mediated adsorption model for the condensation of water vapor at an ice surface can be represented by the following equation:

$$H_2O(g) \underset{k_d}{\overset{k_a}{\rightleftharpoons}} H_2O(ad) \underset{k_{-r}}{\overset{k_r}{\rightleftharpoons}} H_2O(s) \quad (6)$$

In these equations, $H_2O(g)$ is the gas-phase water molecule, $H_2O(ad)$ is the precursor adsorbed species, and $H_2O(s)$ represents the H_2O molecule that has been incorporated into the ice surface. k_a and k_d are the adsorption and desorption rate constants. k_r and k_{-r} are the rate constants for the reaction of the H_2O precursor into and out of the ice surface.

The overall rate of adsorption into the precursor state can be defined by the equation $k_a[H_2O(g)] = \sigma\Phi$. In this equation, σ is the trapping coefficient, which represents the probability that an H_2O molecule colliding with the ice surface will be trapped into the physisorbed precursor state. Likewise, Φ represents the H_2O collision rate at the ice surface. After introducing the steady-state approximation, $d[H_2O(ad)]/dt = 0$, the condensation coefficient can be defined according to the equation

$$\alpha = \frac{\sigma}{1 + (k^0_d/k^0_r)\exp[-(E_d - E_r)/RT]} \quad (7)$$

where k_d and k_r are represented in Arrhenius form where $k_d = k^0_d \exp[-E_d/RT]$ and $k_r = k^0_r \exp[-E_r/RT]$. Equation 7 indicates that the condensation coefficient is dependent upon the kinetics of the two competing mechanisms which deplete the precursor state.

Equation 7 can be used to fit the experimental condensation coefficient. Figure 6 displays the best fit to the experimental data that was obtained with $\sigma = 1.06$, $k^0_d/k^0_r = 1.0$, and $E_d - E_r = 0.23$ kcal/mol. The uncertainty in these values was $k^0_d/k^0_r = 1.0 \pm 0.1$ and $E_d - E_r = 0.23 \pm 0.03$ kcal/mol. These best-fit parameters suggests that the kinetics for desorption and reaction from the physisorbed precursor state of H_2O on ice are nearly equivalent to one another. The equivalence of the preexponential factors also indicates that the transition states for desorption and reaction are similar. Assuming that reaction represents the diffusion of H_2O on the ice surface, this equality suggests that the similar transition states for desorption and diffusion may be a two-dimensional gas.

The existence of an H_2O precursor may also be consistent with the suggestion by Faraday[60] that a "liquidlike" layer exists on ice surfaces. Although the presence of such a liquidlike layer on ice

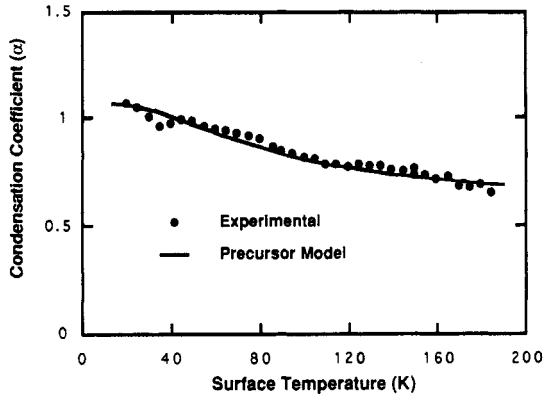

Figure 6. Fit of the precursor-mediated adsorption model to the condensation coefficient for H_2O on ice as a function of ice surface temperature.

has not been verified by direct means,[61] a number of indirect investigations have suggested its presence. Evidence for a liquid layer on ice was provided by Davy and Somorjai[6] while examining the vaporization of H_2O from single-crystal ice surfaces at fairly high temperatures from 183 to 233 K.[6] This study concluded that there may be a highly mobile H_2O species on the ice surface at temperatures above 213 K, which is hydrogen-bonded to only one nearest neighbor.[6] This precursor H_2O species was believed to be the source of the desorbed H_2O molecules during vaporization. This mobile, weakly bound molecule could also be the precursor to adsorption.

Condensation coefficients that decrease as a function of surface temperatures can also be predicted by a single-collision surface trapping model.[62] In this model, an incoming gas molecule collides with the surface. This collision results in momentum transfer from the incident gas molecule to the surface. Trapping of an incident gas molecule occurs when the incident molecule transfers enough momentum that its kinetic energy is insufficient to escape the surface potential. Under the appropriate conditions, less momentum transfer and a lower sticking coefficient are predicted at higher surface temperatures.[62]

Recent theoretical modeling for Ar on Pt(111)[63] also provides a physical picture that illustrates the effect of surface temperature. The calculations show rapid equilibration for the normal component of argon's velocity on Pt(111) and much slower equilibration for the parallel velocity component. At elevated surface temperatures, the Ar residence time is decreased and desorption occurs before the parallel component can equilibrate with the surface. Consequently, there is decreased adsorption at higher surface temperatures in agreement with the precursor-mediated adsorption kinetic model.[63]

B. Evaporation Coefficient. Equation 2 defines the evaporation coefficient, γ, as the experimental rate of evaporation, E_{exp}, divided by the maximum theoretical rate of evaporation, E_{max}. The vapor pressure, P_s, must be defined to obtain the maximum theoretical rates of evaporation versus temperature. The standard procedure is to assume that P_s is equivalent to the equilibrium vapor pressure of ice at the given surface temperature, T_s. These equilibrium vapor pressures were determined directly by the steady-state experimental results for the surface temperature and vapor pressure displayed in Figure 4.

The experimental rates of evaporation, dx/dt, versus temperature were obtained from temperature-dependent interference measurements such as those shown in Figure 3. In the case of evaporation

$$dx/dt = -\gamma P_s/[\rho(T)(2\pi mkT_s)^{1/2}] \quad (8)$$

where γ denotes the evaporation coefficient and all other symbols have been defined previously. Equation 7 can be rearranged to solve for γ in terms of dx/dt, P_s, $\rho(T)$, and T. The evaporation coefficients versus temperature are displayed in Figure 7.

The evaporation coefficients were essentially constant over the measured temperature range with an average value of $\gamma = 0.63 \pm 0.15$. There is a large disparity between this value and the majority of the evaporation coefficients shown in Table I, which are an order of magnitude lower. However, most of the evaporation studies displayed in Table I represent evaporation from liquid water. The single measurement of the evaporation coefficient for ice was from a very early previous investigation that obtained a slightly larger value of $\gamma = 0.94 \pm 0.06$ between 188 and 213 K.[2]

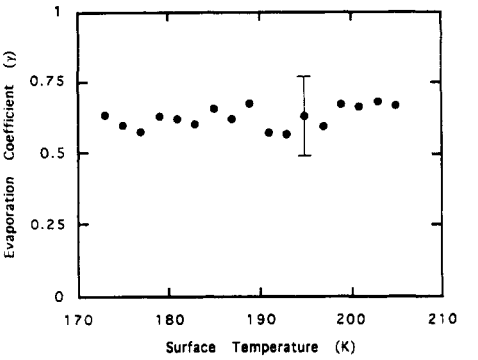

Figure 7. Evaporation coefficient for H_2O from ice as a function of ice surface temperature.

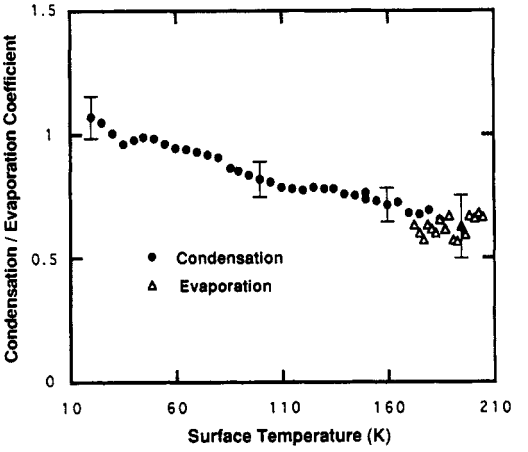

Figure 8. Comparison between the measured condensation and evaporation coefficients.

C. Comparison of Condensation and Evaporation Coefficients. This investigation is the first study in which condensation and evaporation coefficients of H_2O on ice surfaces have been measured by the same technique. Figure 8 displays the comparison between the condensation coefficients from Figure 5 and the evaporation coefficients from Figure 7. Figure 8 reveals that the previously assumed equivalency between condensation and evaporation coefficients[1-3,12,18,19,23-29] is correct within the error limits of these experiments. One previous study has obtained both evaporation and condensation coefficients of H_2O on liquid water surfaces.[22] This earlier study determined that the evaporation and condensation coefficients of H_2O on liquid water surfaces are nearly equivalent and $\alpha = \gamma = 1.0$.[22]

The equivalence of the condensation and evaporation coefficients indicates that condensation and evaporation can be considered separately during net condensation, net evaporation, or steady-state equilibrium. The incoming H_2O vapor flux does not interfere with desorbing H_2O molecules up to H_2O vapor pressures of at least 1×10^{-4} Torr. The equivalency also suggests that evaporative cooling and condensative heating of the ice surface are negligible. Evaporation does not reduce desorption rates by the cooling of the ice surface. Likewise, impinging H_2O molecules do not induce the evaporation of surface H_2O molecules through a surface heating mechanism.

The observed equivalence of the condensation and evaporation coefficients also indicates that the condensation of the incoming H_2O vapor phase is probably independent of vapor temperature up to 300 K. This proposed temperature independence may be

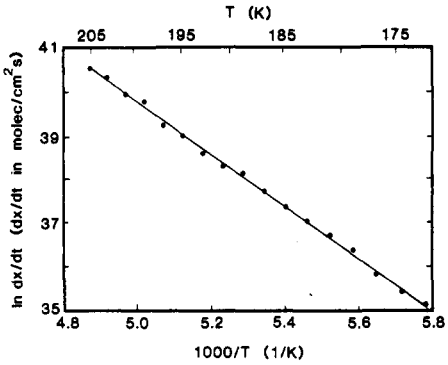

Figure 9. Arrhenius plot of the isothermal H_2O desorption rates from an ice surface.

attributed to the efficient dissipation of the kinetic energy of the vapor by the ice crystal lattice. The equivalence also suggests that the ice surface structure does not influence condensation and evaporation. Vitreous ice and ice I are both formed at their respective temperatures[52] over the 20–185 K temperature range of the condensation coefficient experiments. The condensation coefficients shown in Figure 5 do not display any discontinuities that may be associated with different surface structures. Likewise, Figure 7 does not manifest any evidence of reconstructions of the ice surface that may occur as a result of evaporation in the temperature range from 173 to 205 K.

D. Isothermal Desorption Kinetics. The sinusoidally varying interference signals observed in Figure 3 indicate a constant desorption rate at each temperature. This behavior provides evidence for zero-order desorption kinetics. Zero-order kinetics are expected in multilayer desorption. For zero-order kinetics, the isothermal desorption rate is

$$d\theta/dt = \nu_0 e^{-E_d/RT_s} \tag{9}$$

where θ is the coverage in units of molecules per centimeter squared. All other symbols have been previously defined.

Figure 9 shows the Arrhenius plot of the isothermal desorption rates obtained from the isothermal desorption experiments. The slope of a linear fit to this plot yielded a desorption activation barrier of $E_d = 11.9 \pm 0.2$ kcal/mol. The intercept produced a zero-order preexponential of $\nu_0 = 2.8 \times 10^{30} \pm 1.0 \times 10^{30}$ molecules/(cm^2 s). The magnitude of this preexponential is characteristic of zero-order multilayer desorption.[48] The desorption activation barrier is also in agreement with previous temperature-programmed desorption studies of ice multilayers on metal surfaces,[64] which have measured $E_d = 11.5$ kcal/mol.[65,66]

E. Quasi-Equilibrium Measurements. The term quasi-equilibrium indicates that the isosteric experiments are performed under steady-state conditions but not true equilibrium conditions. Under true equilibrium conditions, the gas temperature, T_g, and the surface temperature, T_s, are equal. However, the difference between true equilibrium and quasi-equilibrium conditions has previously been shown to be negligible.[67] Consequently, the analysis of quasi-equilibrium measurements generally proceeds as if the measurements were performed at true equilibrium.

For the equilibrium between a gas and its solid, the equilibrium at any temperature is characterized by the vapor pressure:

$$K_{eq} = P_v = \exp[-\Delta G_{sub}/RT] \tag{10}$$

In this expression, K_{eq} is the equilibrium constant, ΔG_{sub} is the free energy of sublimation, and $\Delta G_{sub} = \Delta H_{sub} - T\Delta S_{sub}$ where ΔH_{sub} is the enthalpy of sublimation and ΔS_{sub} is the entropy of sublimation. Rearrangement of this relationship yields the slope–intercept form of the Clausius–Clapyron equation:

$$\ln (P_v) = -\Delta H_{sub}/RT + \Delta S_{sub}/R \tag{11}$$

The enthalpy of sublimation, ΔH_{sub}, and the entropy of sublimation, ΔS, may be obtained by fitting eq 11 to the data in Figure 4. The resultant ln (P_v) vs $1/T$ plot is shown in Figure 10 with P_v in atmospheres. This plot yields a slope corresponding

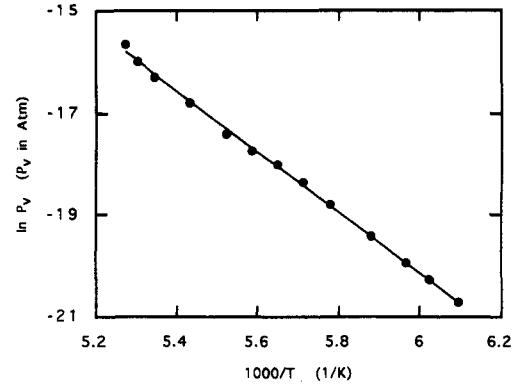

Figure 10. Clausius–Clapyron equation displaying the relationship between the ice surface temperature and H_2O vapor pressure necessary to maintain a constant ice coverage. The slope yields $\Delta H_{sub} = 11.8 \pm 0.2$ kcal/mol and the y-intercept gives $\Delta S_{sub} = 31.0$ cal/(K mol).

TABLE III: Predicted Condensation and Evaporation Rates for H_2O on Ice Surfaces Using Temperatures and H_2O Partial Pressures versus Altitude Obtained from Balloon Measurements over the South Pole during June and July of 1990

altitude, km	temp, °C	H_2O partial pressure, Torr	condensatn rate, ML/s	evaporatn rate, ML/s
5	−35	7.5×10^{-2}	30000	39000
7.5	−60	3.5×10^{-3}	1580	1630
10	−70	1.6×10^{-3}	750	410
12.5	−75	4.5×10^{-4}	210	195
15	−82	3.8×10^{-4}	180	65
17.5	−88	2.5×10^{-4}	120	23
20	−93	1.3×10^{-4}	65	10

to $\Delta H_{sub} = 11.8 \pm 0.2$ kcal/mol and a y-intercept value giving $\Delta S_{sub} = 31.0$ cal/K mol.

The value determined for the heat of sublimation is in agreement with the measured value of $\Delta H_{sub} = 12.2$ kcal/mol determined previously by Davy and Somorjai[6] for crystalline ice and $\Delta H_{sub} = 12.2$ kcal/mol for amorphous ice.[68] Similarly, the measured value for the entropy of sublimation is in good agreement to that expected for the addition of the entropy of fusion [$\Delta S_{fus} = 5.3$ cal/(K mol)] and the entropy of vaporization [$\Delta S_{vap} = 26.0$ cal/(K mol)].[52] Within experimental error, the measured value for the enthalpy of sublimation, $\Delta H_{sub} = 11.8 \pm 0.2$ kcal/mol, is also equivalent to the desorption activation energy of $E_d = 11.9 \pm 0.2$ kcal/mol that was determined by the isothermal desorption experiments. This equivalency between the equilibrium and kinetic values indicates that there is no apparent kinetic barrier for H_2O adsorption on H_2O multilayers.

An approximation for the average hydrogen bond energy in crystalline ice can be derived if the intermolecular binding energy of the H_2O lattice is attributed to hydrogen bonding. Because each H_2O molecule in the crystal lattice participates in two hydrogen bonds, the strength of each hydrogen bond may be determined by dividing the enthalpy of sublimation by two:

$$E_{H\text{-bond}} = \Delta H_{sub}/2 \tag{12}$$

Applying this definition and using $\Delta H_{sub} = 11.8$ kcal/mol, we derive an average hydrogen bond energy of $E_{H\text{-bond}} = 5.4$ kcal/mol for temperatures between 164 and 190 K. This hydrogen bond energy compares favorably with $E_{H\text{-bond}} = 5.66$ kcal/mol obtained from relevant thermodynamic data for ice I at 0 K.[52]

F. Relevance to Heterogeneous Atmospheric Chemistry. Polar stratospheric clouds (PSCs) are ice particles in the polar stratosphere at altitudes of 10–20 km.[69] Heterogeneous chemistry on PSCs has recently been suggested as a mechanistic step in the catalytic destruction of ozone over Antarctica.[15-17] Although the presence of these ice particles over the polar regions is well documented, modeling of PSC growth and stability is contingent upon accurate values for the condensation and evaporation rates for H_2O on ice.[70] In this study, the rates of condensation and evaporation have been accurately determined as a function of temperature. Under the assumption that particle nucleation will

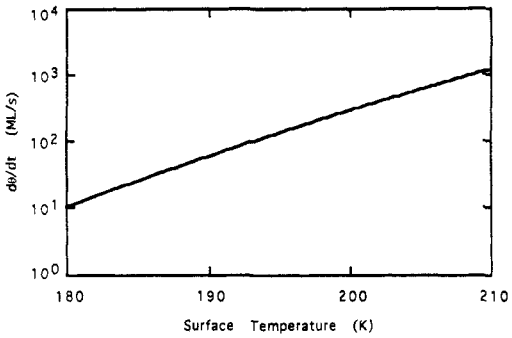

Figure 11. H_2O desorption rates from ice as a function of ice surface temperature between 180 and 210 K where ice particles are observed in the polar stratosphere. At equilibrium, the H_2O desorption rates are equal to the H_2O adsorption rates.

occur, these rates can be used to estimate the altitude of PSC formation.

Table III displays an example of condensation and evaporation rates for representative conditions over the Antarctic Pole. Temperature and H_2O partial pressure values versus altitude used in Table III were obtained during balloon-borne measurements over the South Pole in 1990.[71] This table indicates that PSCs are not expected at altitudes <10 km because condensation rates are smaller than evaporation rates. In contrast, PSC growth is predicted for >10 km, where condensation rates are larger than evaporation rates. These results are in excellent agreement with the concurrent balloon-borne backscatter measurements, which observed ice PSCs at altitudes between 12.5 and 20 km.[71]

The evaporation and condensation rates given in Table III also reveal the dynamic character of the PSC surface under typical stratospheric conditions. The rates indicate that the ice surface is not static but is constantly desorbing and adsorbing H_2O molecules. Figure 11 displays the predicted adsorption and desorption rates as a function of temperature for an ice surface in equilibrium with H_2O vapor. Adsorption and desorption rates of 10–1000 ML/s are observed over the stratospheric temperature range from 180 to 210 K under equilibrium conditions. One monolayer (ML) is defined according to the solid density of ice at 193 K; i.e., 1 ML = $\rho^{2/3}$ = 9.8 × 10^{14} H_2O molecules/cm^2. This definition does not consider the bilayer structure of ice.

The finite lifetime of the ice surface may have important implications for heterogeneous atmospheric chemistry.[15] For example, one reaction that occurs on PSCs and has received considerable attention because of its role in the "ozone hole" is

$$ClONO_2 + H_2O \rightarrow HOCl + HNO_3 \qquad (13)$$

This PSC reaction takes a stable chlorine reservoir molecule, $ClONO_2$, and converts it into a photochemically active chlorine molecule, HOCl. Whether this reaction occurs on the ice surface or in the ice bulk is not known. However, the ice surface of a PSC is constantly changing as H_2O molecules desorb and adsorb. Adsorbing H_2O molecules may quickly solvate and subsequently encapsulate the reactant $ClONO_2$ molecules in an ice matrix. Consequently, PSC reactions may occur in the ice bulk rather than on ice surfaces.

The constant flux of adsorbing and desorbing H_2O molecules at 10–1000 ML/sec may also affect the evolution of reaction products. For example, the HOCl reaction products may be generated in the ice bulk and may require H_2O desorption to "uncover" them before they can be desorbed. On the other hand, if the HOCl products are generated on the ice surface, they may be quickly solvated by incident H_2O molecules and trapped in an ice matrix. The desorption of HOCl products from the ice surface would then be dependent on the prior desorption of the H_2O solvation cages.

The large adsorption and desorption rates from ice particles under stratospheric conditions reveal the dynamic character of the ice surfaces of polar stratospheric clouds. The possible interplay between the H_2O adsorption and desorption kinetics and the heterogeneous reaction kinetics raises important questions in heterogeneous atmospheric chemistry. Understanding the nature of these heterogeneous reactions is a fascinating frontier in ice surface chemistry and will be pursued in future studies.

V. Conclusion

Optical interference techniques were used to measure the condensation coefficients for H_2O on ice surfaces for surface temperatures from 20 to 185 K. The condensation coefficients, α, were observed to decrease with ice surface temperature from an initial value of $\alpha = 1.06 \pm 0.10$ at 20 K to $\alpha = 0.65 \pm 0.08$ at 185 K. This decrease with surface temperature was consistent with a precursor-mediated adsorption model.

The evaporation coefficients for H_2O from H_2O multilayers were examined at surface temperatures from 173 to 205 K. These isothermal desorption measurements also employed optical interference techniques. The evaporation coefficients were determined to be constant at $\gamma = 0.63 \pm 0.15$ versus temperature between 173 and 205 K. The evaporation coefficients were equivalent to the condensation coefficients within the experimental error limits over the temperature range where they both could be measured. This equivalency indicates that evaporation or condensation do not perturb or alter the ice surface. In addition, evaporation and condensation can be considered independent of one another during net condensation, net evaporation, or steady-state equilibrium.

The isothermal desorption kinetics for H_2O desorption from ice surfaces were also measured using optical interference techniques. An Arrhenius analysis of the isothermal desorption rates versus temperature revealed zero-order desorption kinetics as expected for H_2O multilayer desorption. The activation barrier for desorption was $E_d = 11.9 \pm 0.2$ kcal/mol with a zero-order preexponential of $\nu_0 = 2.8 \times 10^{30} \pm 1.0 \times 10^{30}$ molecules/(cm^2 s).

Quasi-equilibrium optical experiments also determined the enthalpy of sublimation, ΔH_{sub}, and entropy of sublimation, ΔS_{sub}, for H_2O multilayers. The quasi-equilibrium measurements versus temperature yielded $\Delta H_{sub} = 11.8 \pm 0.2$ kcal/mol and $\Delta S_{sub} = 31.0$ cal/K mol. The equivalency of the kinetic desorption activation barrier, E_d, and the enthalpy of sublimation, ΔH_{sub}, indicates that there is no barrier for H_2O adsorption on ice surfaces. The enthalpy of sublimation, ΔH_{sub}, also yields an average hydrogen bond energy in ice of $E_{H\text{-bond}} = 5.4$ kcal/mol.

These results for the condensation and evaporation of H_2O on ice surfaces have important implications for heterogeneous atmospheric chemistry. Adsorption and desorption rates of 10–1000 ML/s are predicted over the stratospheric temperature range from 180–210 K under equilibrium conditions. The ice surface is extremely dynamic and rapid solvation by impinging H_2O molecules may occur on a millisecond time scale. As a result, heterogeneous atmospheric reactions may occur in the ice bulk rather than on a static ice surface.

Acknowledgment. This research was supported by the Office of Naval Research under Contract N00014-92-J-1365. We thank Prof. Margaret A. Tolbert and Prof. Gilbert M. Nathanson for useful discussions. S.M.G. acknowledges the National Science Foundation for a Presidential Young Investigator Award.

Registry No. H_2O, 7732-18-5.

References and Notes

(1) Alty, T.; MacKay, C. A. *Proc. R. Soc. London* **1935**, *149*, 104.
(2) Tschudin, K. *Helv. Phys. Acta* **1946**, *19*, 91.
(3) Kramers, H.; Stremerding, S. *Appl. Sci. Res. A* **1953**, *3*, 73.
(4) Nabavian, K.; Bromley, L. A. *Chem. Eng. Sci.* **1963**, *18*, 651.
(5) Koros, R. M.; Deckers, J. M.; Andres, R. P.; Boudart, M. *Chem. Eng. Sci.* **1966**, *21*, 941.
(6) Davy, J. G.; Somorjai, G. A. *J. Chem. Phys.* **1971**, *55*, 3624.
(7) Chodes, N.; Warner, J.; Gagin, A. *J. Atmos. Sci.* **1974**, *31*, 1351.
(8) Bonacci, J. C.; Myers, A. L.; Nongbri, G.; Eagleton, L. C. *Chem. Eng. Sci.* **1976**, *31*, 609.
(9) Leu, M. *Geophys. Res. Lett.* **1988**, *15*, 17.
(10) Turco, R. P.; Toon, O. B.; Hamill, P. *J. Geophys. Res.* **1989**, *94*, 16493.
(11) Isono, K.; Iwai, K. *Nature* **1969**, *223*, 1149.
(12) Warner, J. *J. Atmos. Sci.* **1969**, *26*, 1272.

(13) Schwartz, S. E. *Chemistry of Multiphase Atmospheric Systems.* In NATO ASI Series Vol. G6; Jaeschke, W., Ed.; Springer-Verlag: Berlin, 1986.
(14) Pruppacher, H. R. *Microphysics of Clouds and Precipitation*; D. Reidel Pub. Co.: Dordrecht, Holland, 1978.
(15) Solomon, S. *Rev. Geophys.* **1988**, *26*, 131.
(16) Molina, M. J.; Tso, T.-L.; Molina, L. T.; Wang, C.-Y. *Science* **1987**, *238*, 1253.
(17) Tolbert, M. A.; Rossi, M. J.; Malhotra, R.; Golden, D. M. *Science* **1987**, *238*, 1258.
(18) Alty, T. *Proc. R. Soc. London A* **1931**, *131*, 554.
(19) Sinarwalla, A. M.; Alofs, D. J.; Carstens, D. J. *J. Atmos. Sci.* **1975**, *32*, 592.
(20) Levine, N. E. *J. Geophys. Res.* **1973**, *78*, 6266.
(21) Wenzel, H. *Int. J. Heat Mass Trans.* **1969**, *12*, 125.
(22) Schulze, F.-W.; Cammenga, H. K. *Ber. Bunsenges. Phys. Chem.* **1980**, *84*, 163.
(23) Alty, T. *Philos. Mag.* **1933**, *15*, 82.
(24) Alty, T.; Nicole, F. H. *Can. J. Res.* **1931**, *4*, 547.
(25) Narusawa, M.; Springer, G. S. *J. Colloid Interface Sci.* **1975**, *50*, 392.
(26) Kiryukhin, B. V.; Plaude, N. O. In *Studies of Clouds, Precipitation and Thunderstorm Electricity*; Vulfson, N. I., Levin, L. M., Eds.; Amer. Meteor. Soc.: Boston, 1965.
(27) Yamamoto, G.; Miura, A. *J. Meteor. Soc. Jap.* **1949**, *27*, 257.
(28) Pruger, W. *Z. Phys.* **1940**, *115*, 202.
(29) Delaney, L. J.; Houston, R. W.; Eagleton, L. C. *Chem. Eng. Sci.* **1964**, *19*, 105.
(30) Hammecke, V. K.; Kappler, E. *Z. Geophys.* **1953**, *19*, 181.
(31) Hirth, J. P.; Pound, G. M. *Condensation and Evaporation*; Progress in Materials Science, Vol. XI; Pergamon: Oxford, 1963.
(32) Pound, G. M. *J. Phys. Chem. Ref. Data* **1972**, *1*, 135.
(33) Tanner, D. W.; Pope, D.; Potter, C. J.; West, D. *Int. J. Heat Mass Trans.* **1968**, *11*, 181.
(34) Tamir, A.; Hasson, D. *Chem. Eng. J.* **1971**, *2*, 200.
(35) Mills, A. F.; Seban, R. A. *Int. J. Heat Mass Trans.* **1967**, *10*, 1815.
(36) Bryson, C. E., III; Cazcarra, V.; Levenson, L. L. *J. Vac. Sci. Technol.* **1974**, *11*, 411.
(37) Fujikawa, S.; Akamatsu, T.; Yahara, J.; Fujioka, H. *Appl. Sci. Res.* **1982**, *38*, 363.
(38) Tolbert, M. A.; Middlebrook, A. M. *J. Geophys. Res.* **1990**, *95*, 22423.
(39) Hollenberg, J. L.; Dows, D. A. *J. Chem. Phys.* **1961**, *34*, 1061.
(40) Groner, P.; Stolkin, I.; Gunthard, H. H. *J. Phys. E* **1973**, *6*, 122.
(41) Sugawara, K.; Yoshimi, T.; Okuyama, H.; Shirasu, T. *J. Electrochem. Soc.* **1974**, *121*, 1233.
(42) Rosetti, R.; Brus, L. E. *J. Chem. Phys.* **1980**, *73*, 572.
(43) Olson, G. L.; Kokorowski, S. A.; McFarlane, R. A.; Hess, L. D. *Appl. Phys. Lett.* **1980**, *37*, 1019.
(44) Murakam, K.; Tohmiya, Y.; Takita, K.; Masuda, K. *Appl. Phys. Lett.* **1984**, *45*, 659.
(45) Haynes, D. R.; Helwig, K. R.; Tro, N. J.; George, S. M. *J. Chem. Phys.* **1990**, *93*, 2836.
(46) Tro, N. J.; Arthur, D. A.; George, S. M. *J. Chem. Phys.* **1989**, *90*, 3389.
(47) Tro, N. J.; Nishimura, A. M.; George, S. M. *J. Phys. Chem.* **1989**, *93*, 3276.
(48) Tro, N. J.; George, S. M. *Surf. Sci.* **1988**, *199*, L246.
(49) Poppa, H.; Moorhead, D.; Heinemann, K. *Thin Solid Films* **1985**, *128*, 251.
(50) Tro, N. J.; Haynes, D. R.; Nishimura, A. M.; George, S. M. *J. Chem. Phys.* **1989**, *91*, 5778.
(51) Winkler, A.; Rendulic, K. D.; Wendl, K. *Appl. Surf. Sci.* **1983**, *14*, 209.
(52) Eisenberg, D.; Kauzmann, W. *The Structure and Properties of Water*; Oxford University Press: New York and Oxford, 1969.
(53) Hare, D. E.; Sorensen, C. M. *J. Chem. Phys.* **1986**, *84*, 5085.
(54) Hare, D. E.; Sorensen, C. M. *J. Chem. Phys.* **1987**, *87*, 4840.
(55) Gupta, P.; Coon, P. A.; Koehler, B. G.; George, S. M. *J. Chem. Phys.* **1990**, *93*, 2827.
(56) Gupta, P.; Mak, C. H.; Coon, P. A.; George, S. M. *Phys. Rev. B* **1989**, *40*, 7739.
(57) Weinberg, W. H. In *Kinetics of Interface Reactions*; Grunze, M., Kreuzer, H. J., Eds.; Springer-Verlag: New York, 1987; p 94.
(58) King, D. A.; Wells, M. G. *Proc. R. Soc. London* **1974**, *Ser. A 339*, 245.
(59) Cassuto, A.; King, D. A. *Surf. Sci.* **1981**, *102*, 388.
(60) Faraday, M. *Philos. Mag.* **1859**, *17*, 162.
(61) Hobbs, P. V. *Ice Physics*; Oxford University Press: Oxford, 1969; p 397.
(62) Steinbruchel, Ch.; Schmidt, L. D. *J. Phys. Chem. Solids* **1973**, *34*, 1379.
(63) Head-Gordon, M.; Tully, J. C.; Rettner, C. T.; Mullins, C. B.; Auerbach, D. J. *J. Chem. Phys.* **1991**, *94*, 1516.
(64) Thiel, P. A.; Madey, T. E. *Surf. Sci. Rep.* **1987**, *7*, 211.
(65) Madey, T. E.; Yates, J. T., Jr. *Surf. Sci.* **1978**, *76*, 397.
(66) Stulen, R. H.; Thiel, P. A. *Surf. Sci.* **1985**, *157*, 99.
(67) Ehrlich, G. *J. Chem. Phys.* **1962**, *36*, 1499.
(68) Fletcher, N. H. *The Chemical Physics of Ice*; Cambridge University Press: 1970.
(69) Goodman, J.; Toon, O. B.; Pueschel, R. F.; Snetsinger, K. G. *J. Geophys. Res.* **1989**, *94*, 16449.
(70) Toon, O. B.; Turco, R. P.; Jordan, J.; Goodman, J.; Ferry, G. *J. Geophys. Res.* **1989**, *94*, 11359.
(71) Rosen, J. M.; Kjome, N. T.; Oltmans, S. J. *Geophys. Res. Lett.* **1991**, *18*, 171.

A Comparison of Electrochemical and Gas-Phase Decomposition of Methanol on Platinum Surfaces

K. Franaszczuk,[†] E. Herrero,[‡] P. Zelenay,[†] A. Wieckowski,*

Department of Chemistry, University of Illinois, Urbana, Illinois 61801

J. Wang, and R. I. Masel*

Department of Chemical Engineering, University of Illinois, Urbana, Illinois 61801 *(Received: April 10, 1992)*

By using electrochemical and ultrahigh-vacuum (UHV) techniques, combined with an isotope substitution method, it is found that the mechanism of methanol decomposition on platinum in the electrochemical environment is different than that in the UHV. In the UHV, the first step in the decomposition process is the scission of an O–H bond to yield a methoxy intermediate, whereas in the electrochemical environment, the first step is the scission of a C–H bond. The difference in the decomposition mechanism is discussed in terms of differences in the local electric field at the surface and in terms of methanol hydrophobic/hydrophilic interactions in solution. The latter affect methanol–water near-surface conformation and predetermine the destiny of the individual methanolic bonds in the catalytic splitting.

Introduction

Oxidation of methanol on polycrystalline platinum electrodes has been studied extensively.[1-18] Bagotzky et al.[2] postulated that the rate-determining step involved the rupture of the C–H bond in a methyl group to yield a CH_2OH intermediate:

$$CH_3OH \rightarrow CH_2OH + H^+ + e^- \quad (1)$$

In the gas phase, and at low temperature, methanol was found to adsorb molecularly on group VIII metals and to decompose with an increase in temperature via the mechanism shown in Figure 1.[19] First, methanol undergoes O–H bond scission to yield a methoxy (CH_3O) intermediate. Then, the methoxy sequentially decomposes to yield carbon monoxide and hydrogen.

[†] On leave from the Department of Chemistry, Warsaw University, Warsaw, Poland.
[‡] On leave from the Department of Physical Chemistry, University of Alicante, Alicante, Spain.
* Send correspondence to these authors.

0022-3654/92/2096-8509$03.00/0